
Journal Article

Step-cut modification of air-forced heat sink to improve temperature gradient in power semiconductor modules

Sharp, A., Holzenkamp, H., Akinsolu, M.O., Monir, S. and Vagapov, Y.

Recommended citation:

Sharp, A., Holzenkamp, H., Akinsolu, M.O., Monir, S. and Vagapov, Y. (2025), 'Step-cut modification of air-forced heat sink to improve temperature gradient in power semiconductor modules'. In: Proc. 21th IEEE East-West Design and Test Symposium EWDTS 2025, Tbilisi, Georgia, 5-8 Dec. 2025, pp. 1-6. doi: 10.1109/EWDTS67441.2025.11303673. Available at: https://ieeexplore.ieee.org/document/11303673

Step-Cut Modification of Air-Forced Heat Sink to Improve Temperature Gradient in Power Semiconductor Modules

Andrew Sharp
Wrexham University
Wrexham, UK

Henning Holzenkamp
Wrexham University
Wrexham, UK

Mobayode O. Akinsolu
Wrexham University
Wrexham, UK

Shafiul Monir
Wrexham University
Wrexham, UK

Yuriy Vagapov
Wrexham University
Wrexham, UK

Abstract*—The thermal performance of power electronic systems is critically influenced by the ability to maintain uniform temperatures across semiconductor devices. In serially mounted semiconductor arrangements, forced-air cooling often produces a progressive heating effect, causing downstream devices to operate at higher temperatures. This non-uniform thermal loading leads to localised hotspots, accelerated material degradation, and reduced operational reliability. This paper investigates passive geometric optimisation of an air-cooled aluminium heatsink to enhance thermal uniformity across three serially mounted IGBTs. A computational numerical model was developed in ANSYS Fluent, using steady-state simulations and validated by experimental temperature measurements from a physical test rig. The baseline model demonstrated temperature differences across the length of the heatsink of up to 7.85°C at 100W, confirming the presence of a significant temperature gradient. Geometric modifications were evaluated in the form of a step-cut recess in the heatsink fins. The optimised geometry, with recess depths of 31 mm and 14 mm, reduced the temperature difference to 0.43°C under identical operating conditions, representing over 90% improvement compared to the unmodified design. The findings demonstrate that position-specific geometric tailoring of heatsinks offers a cost-effective and manufacturable solution to improve temperature synchronisation in multi-device power systems.

***Keywords*—power electronics, forced air cooling, temperature gradient, semiconductor reliability**

I. INTRODUCTION

The rapid growth of high-power electronic applications, such as electric drives, renewable energy converters, and automotive powertrains, has significantly increased the thermal demands placed on semiconductor switching devices, particularly insulated-gate bipolar transistors (IGBTs). These devices are highly sensitive to thermal stress, with their performance, reliability, and operational lifetime strongly dependent on maintaining safe and uniform junction temperatures. Uneven heat distribution within a module or across multiple modules mounted in series can lead to localised hotspots, accelerated ageing, and premature device failure [1]-[3].

Recent research has explored various strategies to enhance thermal performance, including novel fin geometries [4], integration of advanced materials such as graphene composites [5], the use of phase change materials (PCM) for transient thermal buffering [6], and hybrid active -passive solutions. While many approaches demonstrate improvements in average heat transfer rates, very few focus on achieving spatially uniform temperature profiles across serially mounted devices, which is a key factor in ensuring balanced electrical performance and reliability [7].

Existing research into heatsink optimisation primarily targets peak thermal resistance or transient cooling improvements, leaving a gap in systematic methods for achieving temperature uniformity through passive geometric modifications. Addressing this gap requires a novel design approach that adjusts local thermal resistance along the heatsink length to synchronise heat extraction from all modules without increasing system complexity or cost.

This paper proposes a solution based on passive geometric modifications to a standard air-cooled aluminium heatsink, without altering overall dimensions, materials, or airflow parameters, with the goal being to reduce the temperature gradient and hence prolong the life of the semiconductor devices.

II. GEOMETRY AND MATERIAL OF HEATSINK

The heatsink used in this study was based on a physical aluminium heatsink provided by an industrial partner. It forms the foundation of all thermal simulations and serves as the baseline model for optimisation. The geometry was modelled in accordance with the physical structure to allow for accurate comparison and validation of results.

The heatsink was made of Aluminium Al 356 (see Table I), a widely used material in power electronics due to its good thermal conductivity, low weight, and manufacturability [8],[9]. The design consists of a flat baseplate with vertically aligned fins for air cooling and three IGBT modules mounted in series along the baseplate.

Two schematic views of the heatsink geometry are shown in Fig. 1 and Fig. 2. Fig. 1 illustrates the front view, highlighting the fin structure of the validation model. Fig. 2 shows the top view, including the layout and spacing of the three IGBT modules. The dimensions used in the simulation are summarised in Table II. These values reflect the real-world setup and were implemented directly in the ANSYS model.

Validation was a critical part of the simulation workflow, particularly when the objective is to ensure that the numerical model accurately reflects the thermal behaviour of a real physical system. In this instance, the purpose of the validation process was to confirm that the ANSYS Fluent simulations reliably replicate the thermal performance of the heatsink and IGBT setup used in the physical test rig at the university laboratory [10].

979-8-3315-5918-2/25/$31.00 ©2025 IEEE

TABLE I. MATERIAL PROPERTIES OF ALUMINIUM AL356.

Parameter	Description	Value
Density	Mass per unit volume	2670 kg/m^3
Specific Heat Capacity	Heat required to rase temaparure	936 J/(kg·K)
Thermal Conductivity	Heat transfer rate	151 W/(m·K)

The validation strategy followed a two-fold approach. First, temperature data from a physical test rig, assembled and instrumented under controlled conditions, was used to provide a reference dataset that reflected the actual thermal response of the heatsink when exposed to known power inputs and airflow. Second, a dedicated numerical validation model was constructed in ANSYS Fluent to replicate the physical heatsink as closely as possible. The model was configured to match the heatsink geometry, material properties, boundary conditions, and applied power levels used in the experiment.

By comparing temperature readings from the experimental results with the simulation results extracted at equivalent locations, the accuracy of the numerical model could be evaluated. This comparison formed the basis for verifying the reliability of the simulation results and ensured that subsequent design modifications and optimisation efforts were grounded in a validated thermal model.

This Computational Fluid Dynamics (CFD) model was constructed to match the physical test rig as closely as possible and served as the reference for both validation and subsequent design optimisation. The CFD model included the full heatsink geometry with a longitudinal symmetry cut, mirrored airflow setup, and appropriate material properties and boundary conditions.

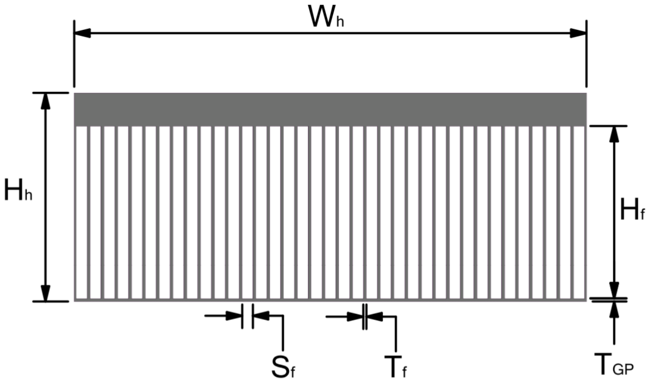

Fig. 1. Front view of heatsink.

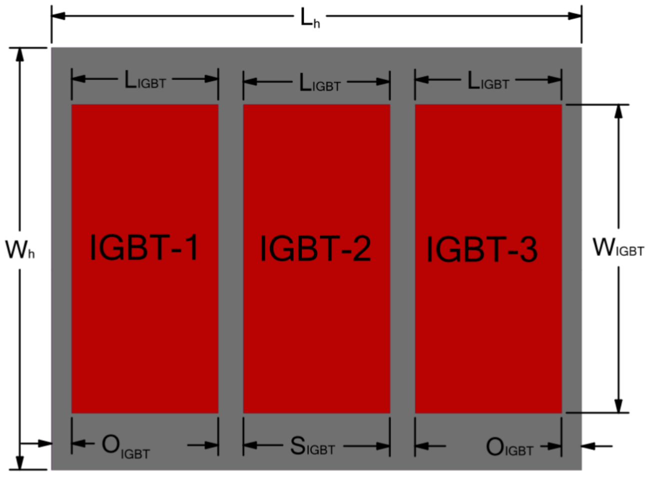

Fig. 2. Top view of heatsink.

TABLE II. DIMENSIONS OF HEATSINK AND IGBT MODULES.

Parameter	Description	Value
L_h	Heatsink length	310 mm
W_h	Heatsink width	167 mm
H_h	Heatsink height	68 mm
H_f	Fin height	56.2 mm
T_f	Fin thickness	1 mm
S_f	Fin spacing	3.5 mm
T_{GP}	Guide plate thickness	1 mm
L_{IGBT}	IGBT-Module length	58 mm
W_{IGBT}	IGBT-Module width	122 mm
S_{IGBT}	IGBT-Module spacing	10 mm
O_{IGBT}	IGBT-Module offset from heatsink edge	8 mm

For comparison with experimental measurements, temperature data were extracted using ANSYS Fluent's surface integral tool. Temperatures were calculated on the surface regions where the IGBT modules interface with the heatsink, corresponding to the thermocouple positions in the physical test rig. This allowed for a consistent comparison between the simulated and measured steady-state temperatures under identical power inputs.

No modifications were applied to the benchmark model at this stage, ensuring that the validation results reflected the unaltered thermal performance of the original heatsink design. All later heatsink modifications were made on the basis of this validated baseline model.

Each IGBT was modelled as a heat-generating source with variable power levels (50 W to 100 W) and mounted directly onto the baseplate of the heatsink. This setup strikes a balance between realism and computational efficiency, enabling effective analysis of thermal behaviour while keeping the simulation computationally manageable.

III. BENCHMARK SIMULATION RESULTS

The baseline simulation was performed using the validated heatsink geometry without any modifications. All simulation conditions, including material properties, boundary setup, and power levels ranging from 50 W to 100 W, were kept consistent to ensure comparability with the later design variations.

Fig. 3 illustrates the steady-state surface heat distribution across the heatsink. The results clearly show thermal accumulation in the central region, confirming uneven cooling performance. A distinct ΔT is visible from the inlet to the outlet, with the highest temperatures forming downstream as the airflow heats up along its path.

TABLE III. SIMULATION RESULTS FOR THE BENCHMARK MODEL.

Power (W)	IGBT1 (°C)	IGBT2 (°C)	IGBT3 (°C)	ΔT (°C)
50	36.48	38.29	40.45	3.96
60	38.61	41.03	43.32	4.71
70	40.68	43.59	46.10	5.41
80	42.80	46.35	48.93	6.13
90	44.47	48.47	51.44	6.97
100	46.83	51.53	54.68	7.85

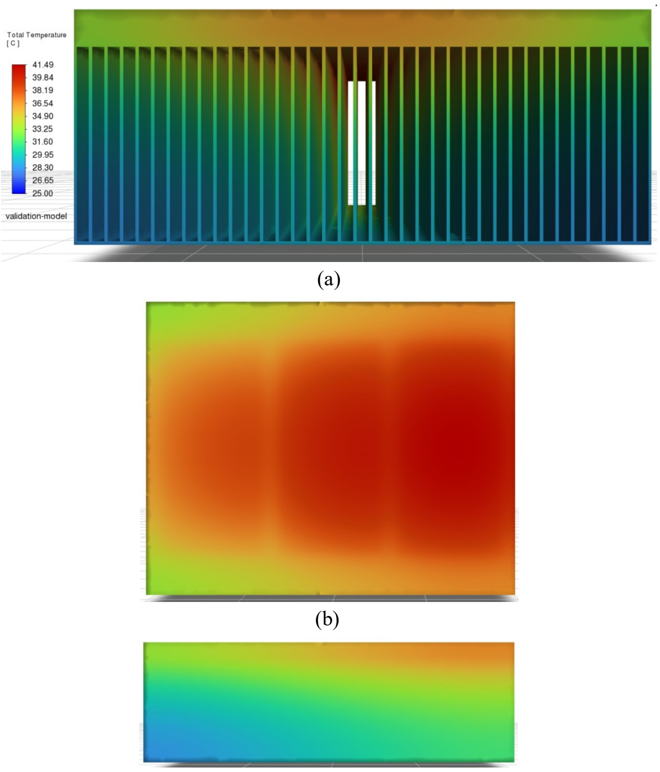

Fig. 3. Thermal distribution in the benchmark model:
(a) front view; (b) top view; (c) side view.

The temperature difference between IGBT3 and IGBT1, expressed as ΔT, increased consistently with input power. At 50 W, the baseline ΔT reached 3.96°C and rose to 7.85°C for 100W in the simulation (see Table III).

The two variations of the step-cut modification were developed to address the thermal imbalance observed in the unmodified benchmark model. The step-cut aimed to solve this by introducing targeted cuts below each IGBT to provide more uniform cooling across the length of the heatsink.

IV. METHODOLOGY

The thermal analysis was carried out using CFD simulations in ANSYS Fluent 2023 R1 and was based on the Finite Volume Method (FVM), a numerical technique particularly well-suited for modelling fluid flow and heat transfer. The software was chosen for its robustness in handling complex convective cooling scenarios, which are essential for accurately representing the behaviour of the air-cooled heatsink in this study.

A steady-state thermal model was used to simulate continuous operating conditions. This assumes that temperatures and heat fluxes remain constant once thermal equilibrium is reached, making the model ideal for evaluating long-term performance and for comparison with temperature measurements taken from the physical artefact at the university laboratory.

The IGBTs themselves were modelled as surface heat sources, with uniform heat flux applied across the contact area of each module. This simplified approach avoids the complexity of internal semiconductor modelling while still capturing the essential thermal behaviour. Power dissipation values ranging from 50 W to 100 W were used to simulate different operating loads.

Overall, this simulation setup provides a reliable and efficient environment for evaluating and improving the thermal performance of the heatsink through numerical optimisation.

After validating the baseline simulation model against experimental data, taken by physical measurements on a heatsink with the same geometry as the simulation model, a series of geometric modifications were introduced to the heatsink with the aim of improving thermal uniformity across the three IGBT modules. The goal of these design changes was to reduce the temperature difference between the hottest and coolest IGBTs by modifying the thermal resistances in sections of the heatsink nearest the air intake.

All modifications were applied directly to the validated ANSYS Fluent model and simulated under identical boundary conditions and power levels. The performance of each design was evaluated by monitoring the surface temperatures at the same locations as in the baseline model, allowing direct comparison of thermal gradients.

Two types of modifications were investigated in this study: a step-cut modification where the outer walls of the heatsink were left intact, and a step-cut modification that removed the outer walls. Each design iteration was assessed based on its ability to reduce the maximum temperature difference (ΔT) between the IGBT modules, and this was taken as an indicator of temperature gradient improvement. To replicate the thermal behaviour of the heatsink under realistic operating conditions, boundary and initial conditions were defined in ANSYS Fluent.

The simulation was set up as a steady-state thermal model with forced convection, aligned with the physical test rig setup where airflow is actively driven through the heatsink. To reduce computational cost and simulation time, the model was cut in half along its vertical longitudinal plane. A symmetry boundary condition was applied to this face, allowing Fluent to solve only one half of the physical domain. This did not affect the validity of the simulation, as both the geometry and thermal loading were symmetrical. However, this required doubling the heat flux values applied to each IGBT in the simulation to ensure the total heat input matched the real test rig setup.

In the physical test setup, air was blown through the heatsink using a fan on the inlet side. However, in the simulation, air was sucked through the heatsink due to solver limitations. This was achieved by setting a velocity inlet of 5 m/s at the outlet side and a pressure inlet at the entry side, with ambient air temperature defined as 25°C.

Although the flow direction was reversed, the simulated thermal behaviour remained valid because the overall convective heat transfer and airflow rate across the heatsink were preserved. The solver interpreted the negative velocity simply as reversed flow, with no adverse effect on heat distribution accuracy.

The three IGBT modules were modelled as surface heat sources. Heat was applied as a uniform heat flux over the base area of each IGBT, with power levels ranging from 50 W to 100 W.

The step-cut modification introduces two distinct height levels into the fins of the heatsink, creating a stepped geometry beneath the IGBT modules. The goal of this design is to modify the effects of the cooling airflow on the IGBT modules by selectively reducing the fin height beneath them. This approach aims to modify the thermal resistances presented at the different sections of the heatsink and hence reduce the ΔT across the IGBTs.

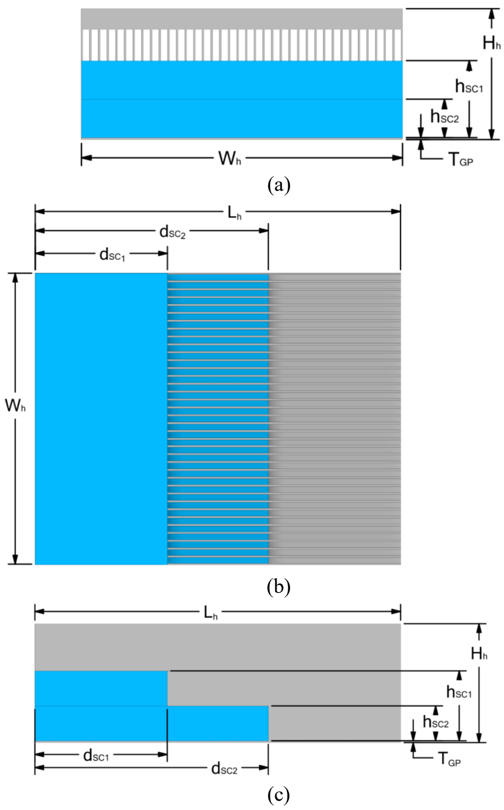

(a)

(b)

(c)

Fig. 4. Geometry of step-cut modification: (a) front view; (b) cut top view of step-cut; (c) cut side view of step-cut.

TABLE IV. DIMENSIONS OF HEATSINK WITH STEP-CUT.

Parameter	Description	Value
L_h	Heatsink length	310 mm
W_h	Heatsink width	167 mm
H_h	Heatsink height	68 mm
T_{GP}	Guide plate thickness	1 mm
d_{SC1}	Step-cut depth	76 mm
d_{SC2}	Step-cut depth	134 mm
h_{SC1}	Step-cut height	20 mm
h_{SC2}	Step-cut height	10 mm

V. STEP-CUT MODIFICATION

The decision for the position and depth of each step was based on the layout of the IGBT modules. The deeper section of the cut was aligned with the border of IGBT1, while the shallower step was aligned with the edge of IGBT2. This positioning allowed a targeted increase of thermal load in the first two modules, which typically exhibit lower temperatures in the baseline model, with an aim to raise the temperature of IGBT1 and IGBT2, by targeted degradation of thermal resistances, to match that of IGBT3.

Fig. 4 shows the geometrical implementation of both configurations, and Table IV. provides the corresponding dimensions. Table V and Table VI show the temperature results for the step-cut modification with and without the outer wall. Both configurations were simulated using identical cut heights of 20 mm and 10 mm. The values include the area-weighted surface temperatures of the three IGBT modules and the corresponding ΔT at each power level from 50 W to 100 W.

All simulations used the same boundary conditions, mesh resolution, and heat flux values as the baseline and previous modification cases. The step depths remained fixed at 76mm and 134mm, respectively, in line with the IGBT layout.

All designs were evaluated under identical thermal and flow boundary conditions, with power inputs ranging from 50 W to 100 W applied to each IGBT. The temperature difference (ΔT) between the hottest and coolest IGBT was used as the metric for evaluating thermal uniformity. Lower ΔT values indicate a more even heat distribution and more balanced cooling. Each configuration was evaluated based on its ability to minimise the ΔT between the IGBT modules, which directly reflects cooling uniformity.

For each case, the absolute temperatures and resulting ΔT values are compared to those of the baseline simulation to assess the effectiveness of the respective geometry.

VI. RESULTS

A. Step-Cut with Outer Fins

Fig. 5 presents the temperature distribution for the step-cut configuration where the outer fins are retained at 50 W input. The resulting ΔT in this configuration was 1.83°C for 50 W power, which is an improvement on the ΔT of 3.96°C of the unmodified baseline model. The retention of the outer fins supports a more controlled and efficient airflow path and represents a 54% improvement in cooling uniformity at 50 W, with a similar percentage improvement at 100 W.

B. Step-Cut without Outer Fins

Fig. 6 shows the thermal distribution of the step-cut heatsink without the outer fin walls at a power input of 50 W. The temperature contour reveals significantly enhanced thermal uniformity across the baseplate, particularly in the region beneath the IGBTs.

The simulation results confirm a ΔT of just 0.37°C, indicating exceptionally balanced heat spread. Compared to the baseline validation case ($\Delta T = 3.96$°C), this represents an improvement of 91% in cooling uniformity at 50 W, with a similar percentage improvement at 100 W.

TABLE V. SIMULATION RESULTS FOR MODIFIED HEATSINK WITH OUTER FINS.

Power (W)	IGBT1 (°C)	IGBT2 (°C)	IGBT3 (°C)	ΔT (°C)
50	39.59	40.88	41.42	1.83
60	42.50	44.05	44.69	2.20
70	45.40	47.22	47.97	2.57
80	48.30	50.38	51.24	2.94
90	51.19	53.55	54.51	3.32
100	54.09	56.71	57.78	3.69

TABLE VI. SIMULATION RESULTS FOR MODIFIED HEATSINK WITHOUT OUTER FINS.

Power (W)	IGBT1 (°C)	IGBT2 (°C)	IGBT3 (°C)	ΔT (°C)
50	40.94	41.33	41.31	0.37
60	44.11	44.59	44.56	0.45
70	47.29	47.84	47.81	0.52
80	50.46	51.09	51.06	0.60
90	53.63	54.34	54.31	0.68
100	56.79	57.59	57.55	0.76

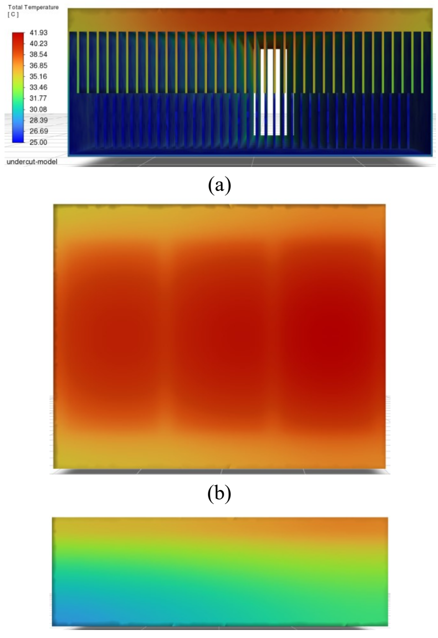

Fig. 5. Thermal distribution for the step cut with outer fins : (a) front view; (b) top view; (c) side view.

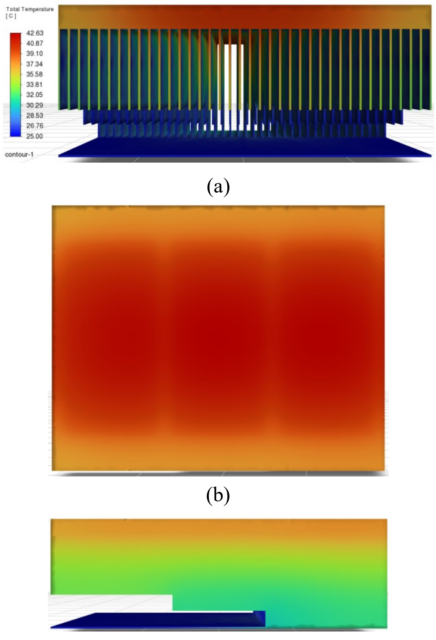

Fig. 6. Thermal distribution for the step-cut without outer fins : (a) front view; (b) top view; (c) side view.

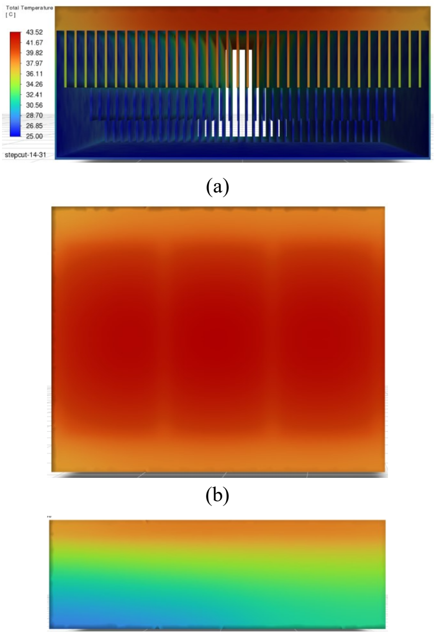

Fig. 7. Thermal distribution for the 31/14mm step-cut : (a) front view; (b) top view; (c) side view.

C. Comparison

Both step-cut configurations significantly reduce the thermal gradient compared to the validated baseline. The step-cut without a wall achieves the lowest ΔT across all power levels, remaining consistently below 1°C even at 100 W. This demonstrates the effectiveness of direct material removal beneath the IGBTs for improving thermal uniformity. The closed-wall version, while exhibiting slightly higher ΔT values, still provides a clear improvement and maintains a more structured airflow channel.

Fig. 8 shows that all designs show an improvement in ΔT trend, which suggests that this approach has the potential to synchronise IGBT temperatures effectively. However, it can be clearly seen that the double step-cut without a wall presents a better result in terms of temperature gradient. This was a critical step toward achieving uniform thermal loading across power modules in real-world applications, and it is this version that is considered further for optimisation.

To identify the most effective geometry for synchronising IGBT temperatures, six different step-cut designs were evaluated under consistent simulation conditions. Each configuration varied in step height and cut depth and was assessed based on its thermal performance under power inputs ranging from 50 W to 100 W. The objective was to minimise ΔT between the three IGBT modules by optimising airflow and heat dispersion beneath the heatsink baseplate.

The comparative progression of ΔT across all tested designs is illustrated in Fig. 9. Each line represents a different step-cut configuration plotted against the power input levels. This graph helps visualise the thermal balancing capabilities of each variant and provides a clear basis for comparison.

Among the tested configurations, the 31/14mm step-cut achieved the most favourable results. It maintained the lowest ΔT across the full power range, starting at just 0.19°C at 50 W and rising gradually to only 0.43°C at 100 W. In comparison, designs such as 40/20mm and 20/10mm reached much higher gradients, with values up to 5.17°C and 3.69°C at 100 W, respectively. The full temperature results for the selected geometry are presented in Table VII.

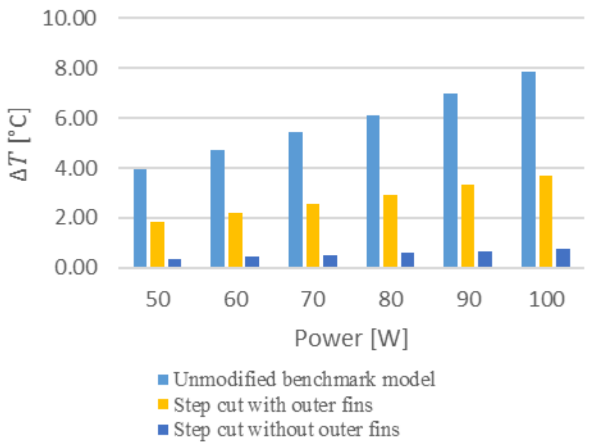

Fig. 8. Comparison of ΔT for the different step-cut modifications.

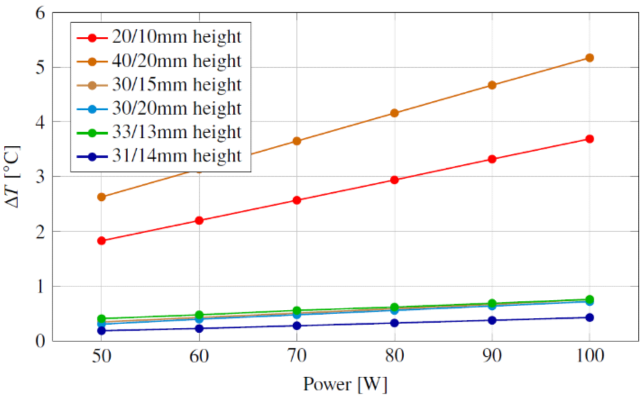

Fig. 9. Comparison of ΔT for different step-cut geometries.

TABLE VI. SIMULATION RESULTS FOR
MODIFIED HEATSINK FOR STEP-CUT SHAPE 31/14 MM.

Power (W)	IGBT1 (°C)	IGBT2 (°C)	IGBT3 (°C)	ΔT (°C)
50	41.93	42.33	42.12	0.19
60	45.31	45.78	45.54	0.23
70	48.67	49.23	48.95	0.28
80	52.03	52.69	52.36	0.33
90	55.39	56.13	55.77	0.38
100	58.75	59.58	59.18	0.43

VII. OPTIMISATION OF STEP-CUT GEOMETRY

To visually support the numerical results, the thermal distribution of the 31/14 mm configuration at 50 W is shown in Fig. 7, which includes four perspectives: isometric, top, front, and side views. The isometric view provides an overall spatial impression of the temperature field across the entire heatsink, revealing balanced heat spread and consistent cooling. The top view illustrates the thermal behaviour directly above the IGBT modules and confirms that surface temperatures are nearly uniform. The front view visualises the internal airflow paths through the fin array, showing smooth vertical gradients and no signs of flow stagnation. Lastly, the side view offers insight into how the step-cut geometry distributes cooler inlet air beneath the baseplate and toward the rear, helping maintain a uniform temperature across all three modules.

The combined data and thermal images confirm that the 31/14 mm geometry delivered highly uniform cooling performance. The small and stable ΔT progression across the full load range demonstrates that this design effectively synchronised IGBT temperatures. Its dimensions allowed for efficient airflow under the heat sources without compromising structural integrity or introducing excessive manufacturing complexity. Compared to other candidates such as 30/15 mm and 33/13 mm, which also performed well, the 31/14 mm cut showed consistently lower ΔT values and smoother performance trends. For these reasons, the 31/14 mm step-cut was selected as the final geometry for continued development and further analysis.

VIII. CONCLUSION

This paper aimed to achieve a uniform heat distribution across three serially mounted IGBT modules positioned on a shared heatsink surface by making a modification to a standard heatsink. In many forced convection applications, temperature asymmetry arises due to the progressive heating of the cooling air as it flows across the heatsink. This non-uniformity leads to increased thermal stress on downstream components and reduces overall system reliability. To address this challenge, a validated numerical model was developed in ANSYS Fluent, using experimental data obtained from a physical test rig at the university laboratory.

The unmodified baseline heatsink showed clear temperature gradients along the IGBT arrangement, with ΔT values increasing from 3.96°C at 50 W to 7.85°C at 100 W. This behaviour confirmed the presence of airflow-induced thermal imbalance. To reduce this effect, two variations of the same geometric modifications were introduced to the fins of the heatsink, with the intention to redistribute airflow and alter local thermal conduction in a manner that promotes uniform temperature conditions.

Among the tested designs, the step-shaped geometry, where the outer fins were also removed, with cut depths corresponding to 31 and 14 mm, achieved the most uniform heat distribution. In this case, the temperature difference between the hottest and coolest IGBT module was reduced to 0.43°C at 100 W, representing a reduction of over 90% compared to the baseline model.

The local modification of the fin geometry effectively equalised the thermal conditions by compensating for the uneven cooling potential along the airflow path.

These findings confirm that position-specific structural modifications to a heatsink can be used successfully to equalise thermal behaviour across multiple power modules. The approach is passive, cost-efficient, and adaptable, and does not require changes to airflow rates or external cooling systems. This makes it especially relevant for compact and thermally sensitive power electronic systems where uniform heat distribution is essential for long-term operational stability.

REFERENCES

[1] A. Sharp, S. Monir, Y. Vagapov, and R. J. Day, "Temperature gradient improvement of power semiconductor modules cooled using forced air heat sink," in *Proc. XIV Int. Symp. on Industrial Electronics and Applications*, Banja Luka, Bosnia and Herzegovina, 2022, pp. 1–5, doi: 10.1109/INDEL55690.2022.9965507

[2] C. Bünnagel, S. Monir, A. Sharp, A. Anuchin, O. Durieux, I. Uria, and Y. Vagapov, "Forced air cooled heat sink with uniformly distributed temperature of power electronic modules," *Applied Thermal Engineering*, vol. 199, 2021, Art. no. 117560, doi: 10.1016/j.applthermaleng.2021.117560

[3] A. Mueller, C. Buennagel, S. Monir, A. Sharp, Y. Vagapov, and A. Anuchin, "Numerical design and optimisation of a novel heatsink using ANSYS steady-state thermal analysis," in *Proc. 27th Int. Workshop on Electric Drives*, Moscow, Russia, 2020, pp. 1–5, doi: 10.1109/IWED48848.2020.9069568

[4] J. Kong, B. Gijbels, H. Seto, F. R. Sainz, K. Umetani, and W. Martinez, "Innovation design of heatsink: A comparative study on heatsink structure analysis in power electronics," in *Proc. IEEE Design Methodologies Conference*, Grenoble, France, 2024, pp. 1–5, doi: 10.1109/DMC62632.2024.10812126

[5] N. Wang, Y. Liu, L. Ye, and J. Li, "Highly thermal conductive and light-weight graphene-based heatsink," in *Proc. 22nd European Microelectronics and Packaging Conference and Exhibition*, Pisa, Italy, 2019, pp. 1–4, doi: 10.23919/EMPC44848.2019.8951839

[6] M. I. Hasan and H. L. Tbena, "Enhancing the cooling performance of micro pin fin heat sink by using the phase change materials with different configurations," in *Proc. Int. Conf. on Advance of Sustainable Engineering and its Application*, Wasit-Kut, Iraq, 2018, pp. 205–209, doi: 10.1109/ICASEA.2018.8370982

[7] A. Sharp, J. M. Niedermayer, M. O. Akinsolu, Y. Vagapov, S. Monir and A. Dianov, "Numerical optimisation of air-cooled heat sink geometry to improve temperature gradient of power semiconductor modules," in *Proc. XV Int. Symp. on Industrial Electronics and Applications*, Banja Luka, Bosnia and Herzegovina, 2024, pp. 1–5, doi: 10.1109/INDEL62640.2024.10772679

[8] H. Feng, J. K. Yu, and W. Tan, "Microstructure and thermal properties of diamond/aluminium composites with TiC coating on diamond particles," *Materials Chemistry and Physics*, vol. 124, no. 1, pp. 851–855, Nov. 2010, doi: 10.1016/j.matchemphys.2010.08.003

[9] M. M. A. Baig, S. F. Hassan, N. Saheb, and F. Patel, "Metal matrix composite in heatsink application: Reinforcement, processing, and properties," *Materials*, vol. 14, no. 21, Oct. 2021, Art. no. 6257, doi: 10.3390/ma14216257

[10] A. Sharp, S. Monir, R. J. Day, Y. Vagapov, and A. Dianov, "A test rig for thermal analysis of heat sinks for power electronic applications," in *Proc. IEEE East-West Design and Test Symposium*, Batumi, Georgia, 2023, pp. 1–4, doi: 10.1109/EWDTS59469.2023.10297055